CHEMISTRY OF MATERIALS
Article

Chem. Mater. **2010,** *22,* 2417–2426 2417
DOI:10.1021/cm9031495

Influence of Silica Nanoparticles on the Crystallization Behavior of and Proton Relaxation in Cesium Hydrogen Sulfate

Mikhail Kislitsyn and Sossina M. Haile*

Materials Science, Mail Code 309-81, California Institute of Technology, Pasadena, California 91125

Received March 27, 2009. Revised Manuscript Received February 6, 2010

The influence of nanoparticulate SiO_2 on the crystallization behavior of $CsHSO_4$ from aqueous solution has been quantitatively evaluated using powder X-ray diffraction (XRD) and ^1H magic angle spinning nuclear magnetic resonance (NMR) spectroscopy. It is shown that SiO_2 induces amorphization of a portion of $CsHSO_4$ and crystallization of the otherwise metastable phase II form of $CsHSO_4$. The fraction of amorphized $CsHSO_4$ (as determined from an evaluation of the XRD peak intensity) was found to increase from 0% in the absence of SiO_2 to fully amorphized in the presence of 90 mol % (~70 wt %) SiO_2. Within the crystalline portion of the composites, the weight fraction of $CsHSO_4$ phase III was observed to fall almost monotonically from 100% in the absence of SiO_2 to about 40% in the presence of 70 mol % SiO_2 (from both XRD and NMR analysis). These results suggest a crystallization pathway in which SiO_2 particles incorporate an amorphous coating of $CsHSO_4$-like material and are covered by nanoparticulate $CsHSO_4$-II, which coexists with independently nucleated particles of $CsHSO_4$-III. In composites with small molar fractions of $CsHSO_4$, the entirety of the acid salt is consumed in the amorphous region. At high $CsHSO_4$ content, the extent of amorphization becomes negligible, as does the extent of crystallization in metastable phase II. The phase distribution was found to be stable for over 1 year, indicating the strength of the stabilization effect that SiO_2 has on phase II of $CsHSO_4$.

Introduction

Superprotonic solid acids are compounds such as $CsHSO_4$ and CsH_2PO_4 that display a structural phase transition upon heating to a state in which the oxyanion groups (SO_4, SeO_4, PO_4, or AsO_4) undergo rapid reorientation. The extreme structural disorder facilitates high rates of proton transport and renders such materials viable candidates for fuel cell and other applications.[1−7] Over the past several years, oxide additives (SiO_2, TiO_2, and Al_2O_3)[8−16] and even polymers[17] have been utilized to modify the properties of superprotonic solid acids. It has been observed that the additives dramatically enhance the conductivity in the room temperature phase, by as much as 3 orders of magnitude, whereas the high-temperature phase is less sensitive to the presence of the additives. Indeed, both slight enhancements (e.g., SiO_2 in $CsHSO_4$)[11,16] and slight reductions [e.g., SiO_2 in α-$Cs_3(H_2PO_4)(HSO_4)_2$][12] in proton-transport rates in the superprotonic state have been reported. As a consequence, in almost all cases, the magnitude of the conductivity discontinuity otherwise observed at the superprotonic transition is substantially lowered. Such smoothing of the conductivity behavior can be anticipated to be beneficial in technological applications.

Among superprotonic solid acids, $CsHSO_4$ has received perhaps the most attention as a model material for studying the influence of oxide additives on proton-transport properties. Below the superprotonic transition temperature, $CsHSO_4$ can crystallize in one of two monoclinic phases, both of which have space group $P2_1/c$.

*Corresponding author. Telephone: (626) 395-2958. Fax: (626) 395-8868. E-mail: smhaile@caltech.edu.

(1) Haile, S. M.; Chisholm, C. R. I.; Sasaki, K.; Boysen, D. A.; Uda, T. *Faraday Discuss.* **2007**, *134*, 17–39.
(2) Uda, T.; Boysen, D. A.; Chisholm, C. R. I.; Haile, S. M. *Electrochem. Solid-State Lett.* **2006**, *9*(6), A261–A264.
(3) Uda, T.; Haile, S. M. *Electrochem. Solid-State Lett.* **2005**, *8*(5), A245–A246.
(4) Otomo, J.; Tamaki, T.; Nishida, S.; Wang, S. Q.; Ogura, M.; Kobayashi, T.; Wen, C. J.; Nagamoto, H.; Takahashi, H. *J. Appl. Electrochem.* **2005**, *35*(9), 865–870.
(5) Otomo, J.; Nishida, S.; Takahashi, H.; Nagamoto, H. *J. Electroanal. Chem.* **2008**, *615*(1), 84–90.
(6) Bladergroen, B. J.; Meyer, F.; Pasupathi, S.; Linkov, V. *Int. J. Hydrogen Energy* **2008**, *33*(12), 3031–3035.
(7) Lavrova, G. V.; Russkikh, M. V.; Ponomareva, V. G.; Uvarov, N. F. *Russ. J. Electrochem.* **2005**, *41*(5), 485–487.
(8) Otomo, J.; Wang, S. Q.; Takahashi, H.; Nagamoto, H. *J. Membr. Sci.* **2006**, *279*(1−2), 256–265.
(9) Ponomareva, V. G.; Shutova, E. S. *Solid State Ionics* **2007**, *178* (7−10), 729–734.
(10) Otomo, J.; Shigeoka, H.; Nagamoto, H.; Takahashi, H. *J. Phys. Chem. Solids* **2005**, *66*(1), 21–30.
(11) Shigeoka, H.; Otomo, J.; Wen, C. J.; Ogura, M.; Takahashi, H. *J. Electrochem. Soc.* **2004**, *151*(10), J76–J83.
(12) Ponomareva, V. G.; Shutova, E. S. *Solid State Ionics* **2005**, *176* (39−40), 2905–2908.
(13) Ponomareva, V. G.; Lavrova, G. V. *Solid State Ionics* **2001**, *145* (1−4), 197–204.
(14) Ponomareva, V. G.; Lavrova, G. V.; Simonova, L. G. *Solid State Ionics* **1999**, *119*(1−4), 295–299.
(15) Ponomareva, V. G.; Lavrova, G. V. *Solid State Ionics* **1998**, *106* (1−2), 137–141.
(16) Ponomareva, V. G.; Uvarov, N. F.; Lavrova, G. V.; Hairetdinov, E. F. *Solid State Ionics* **1996**, *90*(1−4), 161–166.
(17) Boysen, D. A.; Chisholm, C. R. I.; Haile, S. M.; Narayanan, S. R. *J. Electrochem. Soc.* **2000**, *147*(10), 3610–3613.

Published on Web 03/22/2010

Upon synthesis from aqueous solutions, the compound typically adopts the phase III structure.[18] Upon moderate heating (330−370 K), it transforms to phase II, with a transformation temperature that depends sensitively on the humidity, heating rate, and sample surface condition.[19] The transition to phase I, the superprotonic phase with tetragonal symmetry, occurs at 414 K. (We follow here the original Russian nomenclature system in which the highest symmetry phase is identified as phase I and lower symmetry phases are designated sequentially as encountered on cooling.) While phase III is the thermodynamically stable phase at room temperature, the reverse transformation on cooling, of phase II to phase III, is extremely slow, and phase II can persist in metastable form at ambient temperatures for long periods of time,[20] though typically not indefinitely.[10]

Introduction of SiO_2 into $CsHSO_4$ has been shown to influence the phase behavior. In particular, there is strong evidence that SiO_2 induces amorphization of the solid acid [as reflected in the broadening of powder X-ray diffraction (XRD) peaks], and it has been proposed that an amorphous interfacial phase forms between the silica and solid acid. On cooling from high temperature, it has further been observed that the transformation from phase II to phase III is highly retarded in the presence of SiO_2, whereas the influence on the phase I to II transformation is minimal. These effects have largely been observed in composites formed using microporous SiO_2 (having nanoscale pores) and subjected to heat treatment at ∼150 − 210 °C prior to characterization so as to achieve infiltration of $CsHSO_4$ into the silica pores.[10,11,13,14,16] As a consequence, it has not been possible to establish whether the modifications to the phase behavior of $CsHSO_4$ are a result of strong chemical interactions between the solid acid and silica, of the high-temperature treatment, or of mechanical stresses resulting from encapsulation. In this work, we investigate the interaction of $CsHSO_4$ with nanoparticulate rather than microporous SiO_2, where the composites are not subjected to high-temperature treatment, with the aim of establishing the nature of the chemical effects on the phase formation in the absence of mechanical and thermal effects. Samples of $CsHSO_4$−SiO_2 composites are obtained from the evaporation of water from aqueous solutions of $CsHSO_4$ in a colloidal suspension of SiO_2 nanoparticles. The phase formation is studied quantitatively using powder XRD and supported by nuclear magnetic resonance (NMR) spectroscopy.

Experimental Procedures

Cesium hydrogen sulfate powders were obtained by precipitation from aqueous solutions of cesium sulfate (Alfa Aesar, 99.99% metal basis) and sulfuric acid (EMD Chemicals, 17.8 M) in which the $Cs:SO_4$ mole ratio was fixed at 1:1. Composites were prepared by evaporation of solutions containing cesium hydrogen sulfate and 10 nm of silicon oxide (30 wt % water colloidal dispersion with 320 m^2/g, Alfa Aesar). The composition was varied from 10 to 90 mol % SiO_2 in 10 mol % increments (Table 1). Hereafter, composite materials are identified using the nomenclature CHS-*xx*, where *xx* is the mole percent of $CsHSO_4$. The resulting powders were dried in an oven (80 °C, 5 h) prior to characterization. For comparative purposes, single-phase (or "neat") $CsHSO_4$ was also synthesized in the form of macroscopic single crystals and examined, both as-synthesized and subsequent to thermal treatment. Specifically, a portion of the material was annealed at 130 °C for 10 h under stagnant air with the objective of obtaining samples composed entirely of phase II.

Table 1. Nominal Compositions of $CsHSO_4$−SiO_2 Composite Samples Prepared in This Work

name	mol % $CsHSO_4$	wt % $CsHSO_4$	vol % $CsHSO_4$
CHS-10	10	29.8	24.5
CHS-20	20	48.9	42.3
CHS-30	30	62.1	55.7
CHS-40	40	71.9	66.1
CHS-50	50	79.3	74.5
CHS-60	60	85.2	81.5
CHS-70	70	89.9	87.2
CHS-80	80	93.9	92.1
CHS-90	90	97.2	96.3

Phase identification was performed by powder XRD using a PANalytical X'pert Pro diffractometer (Cu Kα, 45 kV, 40 mA) over the 2θ range of 5−70°, with a step size of $2\theta = 0.017°$ and dwell time per step of 50 s. Prior to data collection, powders were lightly hand-ground using a mortar and pestle. For each composition, the sample preparation procedures and sample quantities were held identical to facilitate comparison of the absolute X-ray peak intensities. Further quantification of the phases present in the composites was carried out by NMR spectroscopy. Single-pulse magic angle spinning (MAS) NMR spectra were obtained at a spinning rate of 12 kHz using a Bruker DSX 500 at 11.7 T (resonance frequency of 500.23 Hz), with $\pi/2$ pulse lengths of 4 μs. To ensure proportionality between the ^1H MAS NMR peak intensity and the proton content, the repetition delay time was set to 3000 s, many times greater than the reported T_1 relaxation time of 10−100 s for $CsHSO_4$.[21−24] Sample quantities were 0.040−0.130 g, and for completeness, measurements were performed on neat $CsHSO_4$ in addition to the composite samples. Background effects were removed from the data by subtracting from the sample spectra the analogous ^1H NMR spectra of the empty rotor. Chemical shifts are referenced to tetramethylsilane (TMS). All XRD and NMR measurements were performed at room temperature. Spin−lattice relaxation constants (T_1) were also directly obtained using an inversion−recovery (i.e., $\pi-\pi/2$) pulse sequence, where peak intensities, measured by fitting the peak profiles to pseudo-Voigt functions, were evaluated as a function of the recovery time.

(18) Itoh, K.; Ukeda, T.; Ozaka, T.; Nakamura, E. *Acta Crystallogr.* **1990**, *C46*, 358–361.
(19) Belushkin, A. V.; Natkaniec, I.; Pakida, N. M.; Shuvalov, L. A.; Wasicki, J. *J. Phys. C* **1987**, 20671–687.
(20) Chisholm, C. R. I.; Haile, S. M. *Mater. Res. Bull.* **2000**, *35*, 999–1005.
(21) Mizuno, M.; Hayashi, S. *Solid State Ionics* **2004**, *167*(3−4), 317–323.
(22) Damyanovich, A.; Pintar, M. M.; Blinc, R.; Slak, J. *Phys. Rev. B* **1997**, *56*(13), 7942–7946.
(23) Hayashi, S.; Mizuno, M. *Solid State Commun.* **2004**, *132*(7), 443–448.
(24) Compton, M. G.; Maynes, K. C.; Pavelites, J.; Baker, D. B. *Solid State Commun.* **2005**, *136*(3), 138–141.

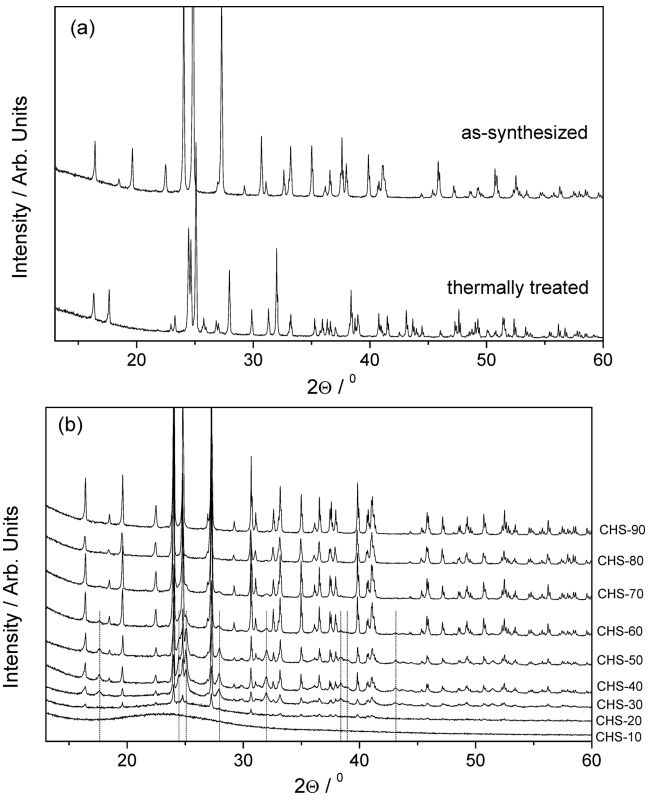

Figure 1. XRD patterns of (a) neat $CsHSO_4$ and (b) composites of $CsHSO_4$ and SiO_2. In part a, the as-synthesized pattern corresponds to phase III and the thermally treated pattern to phase II. In part b, selected peaks uniquely attributable to phase II are indicated.

Results and Data Analysis

Powder XRD. The as-synthesized $CsHSO_4$ (prepared in the absence of SiO_2) was confirmed to be entirely phase III and the annealed material to be entirely phase II (Figure 1a). The diffraction patterns of the as-synthesized composites (Figure 1b) reveal that, in the presence of relatively small amounts of SiO_2, $CsHSO_4$ crystallizes as phase III, as expected. With increasing SiO_2 content, however, phase II also occurs and indeed is the predominant crystalline phase for the sample with 70 mol % SiO_2. This is apparent from the appearance of peaks at, for example, $2\theta = 17.6$ and 32.0° in the higher SiO_2 content compositions, which can only be assigned to phase II. Furthermore, these peaks are significantly broader than those of phase III. It is also evident that, with increasing SiO_2 content in the composite, the total amorphous fraction increases, as reflected in the increasing intensity of a broad amorphous peak centered at $2\theta \sim 23°$. For the highest SiO_2 content sample, no peaks due to crystalline $CsHSO_4$ are evident, despite the nominal $CsHSO_4$ content of almost 30 wt % (10 mol %). A comparison of the patterns obtained from the CHS-40 sample immediately and 1 year after synthesis (Figure 2) shows the two to be identical, indicating that there is insignificant temporal evolution of the phase composition. The behavior contrasts that of neat $CsHSO_4$, in which the (presumably) metastable phase II eventually reverts to phase III.[10]

Quantification of the phase assemblages implied by the diffraction patterns was performed both by Rietveld refinement following background subtraction (see the Appendix) and by direct evaluation of the peak intensities in the raw patterns. To provide a measure of the intensity of the amorphous peak, the integrated intensities of the background profiles were additionally evaluated for the 2θ range of 20−30°. Rietveld refinement was carried out using the commercial software package *X'Pert Plus*, the source code for which is identical to that of the freeware program *Rietica*.[25,26] The structures reported by Chisholm and Haile[20] and by Itoh et al.[18] for phases II and III, respectively, were used as starting models. All crystal chemical parameters (lattice constants, atomic coordinates, etc.) were held fixed during the refinement with the exception of an overall, isotropic atomic displacement parameter for phase II. The peak profiles were treated as asymmetric pseudo-Voigt functions with a full-width at half-maximum (FWHM) that varied with θ according to the Caglioti function $\Gamma = (W + U \tan^2 \theta + V \tan \theta)^{1/2}$ (four refined parameters per phase), and the remaining background was described as a third-order polynomial (four refined parameters). In addition, possible preferred orientation effects were modeled by modifying the intensity of the Bragg peak, P_k, according to $P_k = \exp(P_1 a_k^2)$, where a_k is the acute angle between the scattering vector and the normal to the crystallites (one parameter per phase), and an overall zero shift was refined. The most important refined parameters for the purposes of this study were the scale factors for the two phases, which directly yield the relative amounts of phases II and III in each of the composites. The relevant diffraction data for a typical analysis, specifically the CHS-50 sample, are shown in Figure 3.

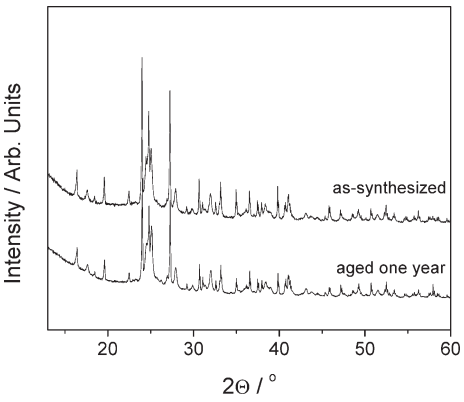

Figure 2. Comparison of the diffraction patterns of freshly synthesized and aged CHS-40.

The results of the refinements for all compositions are summarized in Table 2. As indicated, the final values of the refinement statistics, R_{prof} and R_{Bragg},[27] ranged respectively from 7.3 to 12.3% and from 3.9 to 7.6%. At the highest SiO_2 content, as was already noted, the CHS-10

(25) IUCR. Powder Diffraction **1997**, *22*(21).
(26) Hill, R. J.; Howard, C. J. LHMP1 Program: ANSTO Report M122; Lucas Heights Research Laboratories: Newington, New South Wales, Australia, 1986.
(27) *The Rietveld Method*; Young, R. A., Ed.; International Union of Crystallography; Oxford Science Publications: Oxford, U.K., 1993; p 22.

composite displayed no diffraction peaks due to crystalline $CsHSO_4$. Accordingly, only the results for an analysis of the integrated background intensity are presented for this sample. Because of the high amorphous fraction of the CHS-20 composite (with 80 mol % SiO_2), the phase III/phase II ratio was estimated directly from the ratio of the integrated intensities of selected peaks (the Rietveld refinement suffers from artifacts under such conditions). Consistent with the raw diffraction patterns presented in Figure 2, the phase fraction of phase II generally increases with increasing SiO_2 content up to high concentrations of SiO_2. Specifically, the weight fraction of phase III in the crystalline phase falls almost monotonically from 100% in the presence of 10 mol % SiO_2 to about 40% in the presence of 70 mol % SiO_2. While uncertainty in the phase III/phase II ratio is high for the CHS-20 sample, it is apparent that this sample, displaying a higher concentration of phase III to phase II, deviates from the trend of increasing amounts of phase II with increasing SiO_2 content. Finally, it is noteworthy that the refinement results for the as-synthesized and aged samples are essentially identical for all samples for which the comparative data were collected.

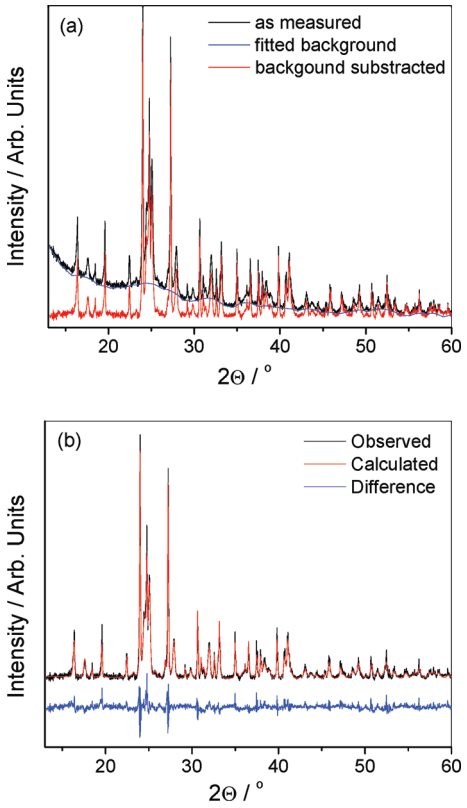

Figure 3. Powder XRD patterns of CHS-50: (a) comparison of raw and background-subtracted patterns; (b) comparison of observed (background-corrected), calculated, and difference patterns, with the latter two obtained from Rietveld refinement.

The Rietveld refinement approach, as implemented here, cannot directly indicate the phase fraction of the amorphous phase, which may differ from the nominal input quantity of SiO_2. Although the measurement of the intensity of the broad amorphous peak does provide some indication of the amorphous content, it is a qualitative rather than a quantitative evaluation. A more direct determination of the amorphous content was performed by evaluating the absolute intensities of the diffraction peaks associated with the crystalline phases of $CsHSO_4$ and comparing them to what would be expected for the case of the complete crystallization of $CsHSO_4$. The analysis was performed as follows. In a uniform mixture of n components and the absence of extinction and microabsorption effects, the absolute intensity of the *hkl* peak of the *i*th phase is given as[28]

$$I_i(hkl) = \frac{K_i(hkl)\,\dfrac{w_i}{\rho_i}}{\sum \mu_i^{\mathrm{m}} w_i} \qquad (1)$$

Table 2. Selected Rietveld Refinement Parameters of the $CsHSO_4$−SiO_2 Composites[a]

sample	R_{exp}, %	R_{prof}, %	R_{Bragg}-II, %	R_{Bragg}-III, %	$R_{w,prof}$ %	wt % phase II	bkgd[b]
CHS-10	n/a	n/a	n/a	n/a	n/a	n/a	11.6(5)
CHS-20	n/a	n/a	n/a	n/a	n/a	20[c]	6.7(5)
aged	*n/a*	*n/a*			*n/a*	*8*[c]	
CHS-30	5.00	7.30	3.90	4.59	9.64	61.0(9)	3.6(5)
aged	*3.44*	*7.38*			*9.63*	*61.4(7)*	
CHS-40	4.90	10.16	6.31	4.69	12.83	47.4(8)	2.7(5)
aged	*3.54*	*8.94*			*11.53*	*49.7(8)*	
CHS-50	6.16	10.13	5.20	5.16	13.10	47.5(3)	0.1(5)
aged	*6.16*	*10.13*			*13.10*	*47.5(3)*	
CHS-60	4.42	9.94	4.59	5.21	12.91	13.7(2)	1.0(5)
aged	*3.43*	*9.20*			*12.15*	*14.1(4)*	
CHS-70	4.52	10.45	6.55	4.57	13.42	4.7(8)	1.2(5)
aged	*3.36*	*9.13*			*12.24*	*3.6(3)*	
CHS-80	5.15	11.56	6.74	6.43	15.01	1.5(9)	0.3(5)
CHS-90	4.59	12.29	n/a	7.61	15.99	< 1	0.5(5)

[a] The refinement statistics R_{exp}, R_{prof}, $R_{w,prof}$, and R_{Bragg} have their usual meanings.[27] [b] The background is the integrated intensity due to the fitted background function over the 2θ range of 20−30°. [c] Rietveld refinement was unreliable because of the low quantity of crystalline $CsHSO_4$ in this sample; the values reported are based on the direct evaluation of the integrated peak intensity at $2\theta \sim 25°$.

where $K_i(hkl)$ is a constant that depends on the nature of the component (e.g., structure factor) and geometry of the XRD system but not on the composition of the mixture, μ_i^m is the mass absorption coefficient of component i, w_i is the weight fraction of component i, and ρ_i is the density of component i. In the present study, nominally three phases occur ($i = 1-3$), and those are $CsHSO_4$-III, $CsHSO_4$-II, and SiO_2 (amorphous). When $I_i(hkl)$ is evaluated relative to the peak intensity obtained from the pure component $I_i^0(hkl)$, the unknown constant $K_i(hkl)$ is eliminated, giving

$$\frac{I_i(hkl)}{I_i^0(hkl)} = \frac{\mu_i^m w_i}{\sum \mu_i^m w_i} \quad (2)$$

This expression is simplified by noting that $\sum w_i = 1$ and that the absorption coefficients of the $CsHSO_4$ phases are identical, to give

$$\frac{I_{CsHSO_4\text{-III}}(hkl)}{I^0_{CsHSO_4\text{-III}}(hkl)} = \frac{W_{CsHSO_4\text{-III}} w_{CsHSO_4} \mu^m_{CsHSO_4}}{w_{CsHSO_4}(\mu^m_{CsHSO_4} - \mu^m_{SiO_2}) + \mu^m_{SiO_2}} \quad (3)$$

where $W_{CsHSO_4\text{-III}}$ is defined as the weight fraction of $CsHSO_4$-III in the crystalline portion of the composite [$= w_{CsHSO_4\text{-III}}/(w_{CsHSO_4\text{-III}} + w_{CsHSO_4\text{-II}})$] and w_{CsHSO_4} is the total weight fraction of crystalline $CsHSO_4$ ($= w_{CsHSO_4\text{-III}} + w_{CsHSO_4\text{-II}}$). Equation 3 could alternatively be written in terms of phase II of $CsHSO_4$ (X-ray peak intensity and weight fraction); however, because $CsHSO_4$-III was the predominant crystalline phase in the majority of the composites, the analysis was performed in terms of this component.

If all of $CsHSO_4$ were to occur in crystalline form (as either $CsHSO_4$-II or $CsHSO_4$-III), then the intensity ratio in eq 3 can be immediately computed using known input quantities: the weight fraction of $CsHSO_4$ (w_{CsHSO_4}) is given directly from the overall composite mixture, the weight fraction of $CsHSO_4$-III in the crystalline portion of the composite ($W_{Cs_2HSO_4\text{-III}}$) is given from the Rietveld refinement, and the absorption coefficients can be computed under the assumption that the amorphous phase has a composition adequately represented as SiO_2. The discrepancy between the measured and computed values of $I_{CsHSO_4\text{-III}}(hkl)/I_{CsHSO_4\text{-III}}{}^0(hkl)$, in particular in cases where the measured value is lower than the computed value, suggests that some of $CsHSO_4$ has not crystallized. The relevant comparison is provided in Figure 4 as a function of the $CsHSO_4$ content, where analysis is performed using the (−1 1 1), (1 1 0), and (0 1 1) diffraction peaks of $CsHSO_4$-III (which have relative intensities of 100, 18.8, and 9.2%, respectively) and the results averaged. It is evident that, for composites with a low total $CsHSO_4$ content, the measured (observed) intensities are lower than the computed (expected) values, indicating the "loss" of some of the crystalline $CsHSO_4$ to amorphization.

The amount of amorphous $CsHSO_4$ was estimated by rewriting eq 2 in terms of four phases, where the additional phase is amorphous $CsHSO_4$ and is taken to have an

(28) Klug, H. P.; Alexander, L. E. *X-Ray Diffraction Procedures for Polycrystalline and Amorphous Phases*, 2nd ed.; John Wiley and Sons: New York, 1974; p 413.

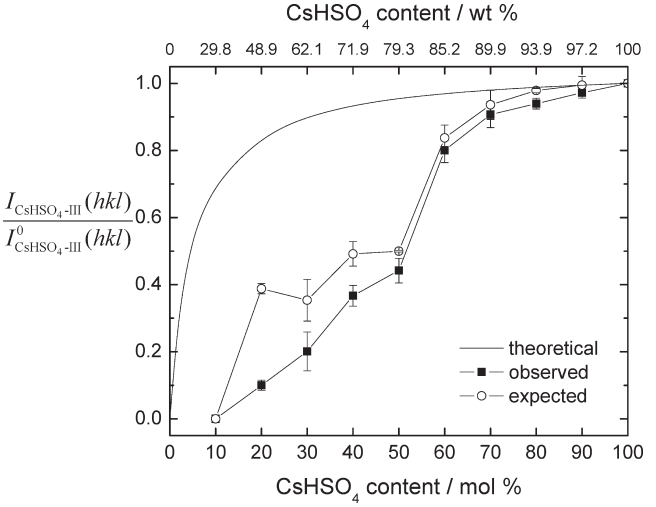

Figure 4. XRD intensity ratios for $CsHSO_4$ phase III (for the intensity in the composites relative to the intensity in neat $CsHSO_4$-III) as a function of the $CsHSO_4$ content. The theoretical curve corresponds to that computed for a simple mixture of $CsHSO_4$-III and SiO_2; the expected data take into account the mixed-phase nature of $CsHSO_4$, and the observed data are taken directly from the diffraction patterns. The difference between the expected and observed data points is attributed to amorphization of a portion of $CsHSO_4$.

Table 3. Weight Percent of $CsHSO_4$ That Is Amorphous (Relative to the Total Amount of $CsHSO_4$ in the System) As Determined by an Evaluation of the Absolute Intensities of the Diffraction Peaks

sample	wt % amorphous	sample	wt % amorphous
CHS-10	100	CHS-60	5
CHS-20	74	CHS-70	3
CHS-30	43	CHS-80	3
CHS-40	25	CHS-90	2
CHS-50	12	CHS-100	0

absorption coefficient equal to that of crystalline $CsHSO_4$. Algebraically, this is simplified by comparing the measured intensity ratio to the "theoretical" intensity ratio for a two-component mixture of $CsHSO_4$-III and SiO_2:

$$\frac{\left(\frac{I_{CsHSO_4\text{-III}}(hkl)}{I^0_{CsHSO_4\text{-III}}(hkl)}\right)^{\text{measured}}}{\left(\frac{I_{CsHSO_4\text{-III}}(hkl)}{I^0_{CsHSO_4\text{-III}}(hkl)}\right)^{\text{theoretical}}} = R = \frac{w_{CsHSO_4\text{-III}}}{w_{CsHSO_4\text{-III}} + w_{CsHSO_4\text{-II}} + w_{CsHSO_4\text{-a}}} \quad (4)$$

where $w_{CsHSO_4\text{-a}}$ is the weight fraction of amorphous $CsHSO_4$ in the system. Using, again, the fact that the sum of all of the weight fractions is 1 and the previously defined quantity $W_{Cs_2HSO_4\text{-III}}$, one obtains the weight fraction of amorphized $CsHSO_4$ as

$$W_{CsH_2SO_4\text{-a}} = \frac{w_{CsHSO_4\text{-a}}}{w_{CsHSO_4\text{-III}} + w_{CsHSO_4\text{-II}} + w_{CsHSO_4\text{-a}}} = 1 - \frac{R}{W_{CsH_2SO_4\text{-III}}} \quad (5)$$

The results (Table 3) indicate that the fraction of $CsHSO_4$ that is amorphized increases monotonically with increasing

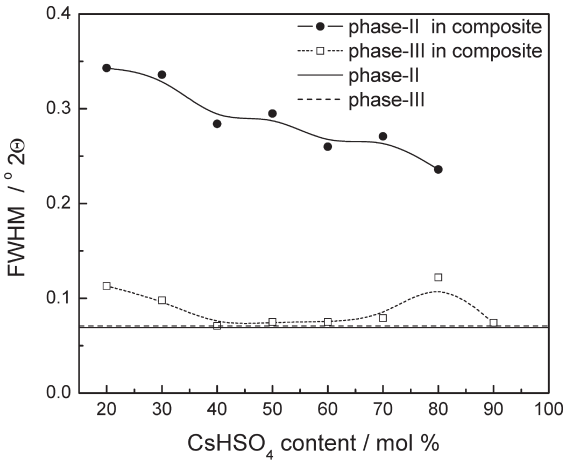

Figure 5. FWHM of the diffraction peak effectively at $2\theta = 40°$ for both phases of $CsHSO_4$ in the composites. The values for neat $CsHSO_4$ are shown as straight lines for comparison.

SiO_2 content, consistent with the overall increase observed in the intensity of the broad amorphous peak with increasing SiO_2 content.

The peak broadening, noted above, is another indicator of the interaction between $CsHSO_4$ and SiO_2. Notably, the broadening is limited to phase II, as is evident in Figure 5, in which the FWHM at $2\theta = 40°$ is plotted as a function of the composite composition for both phases. Peak broadening has been previously reported in the literature on such composite systems.[11,16] The effect has been generally attributed to amorphization of the solid acid phase. What is noteworthy here is that the broadening occurs in addition to amorphization, which causes a reduction in the peak intensities from the $CsHSO_4$ crystalline phases and is responsible for the broad "hump" loosely centered at $2\theta = 24°$. That is, the analysis above implies an amorphous phase that is plausibly independent of structural modifications to crystalline $CsHSO_4$. If the broadening is attributed to a size effect rather than a disordering, the mean particle diameters implied by the Scherrer equation,[29] after taking into account instrumental broadening effects, are 35−45 nm for the crystallites of phase II.

NMR Spectroscopy. The ^1H MAS NMR spectra for $CsHSO_4$ phase II and phase III are shown in Figure 6. In both phases, there is a single crystallographically distinct proton site, and, accordingly, the NMR spectra all show a single peak. The peak is slightly broader for phase III than phase II, suggesting greater local anisotropy in the proton environment of phase III. The chemical shifts are measured to be 11.0 and 12.4 ppm, respectively, and are almost identical with the respective values of 11.2 and 12.6 ppm reported by Hayashi and Mizuno.[23] The shifts measured here further correspond well to the correlation between the O−O distance in the hydrogen bond reported by Eckert et al.:[30]

$$\delta_{iso}/\text{ppm} = 79.05 - 0.255\,(d_{O-H\ldots O})/\text{pm} \qquad (6)$$

Specifically, chemical shifts of 11.9 and 13.9 ppm are expected for the crystallographic distances of 2.636 and 2.555 Å, respectively.[31] The integrated intensities from the two samples are equal within 1%, suggesting that the pulse sequence and delay times employed are sufficient for quantitative phase analysis of the composites. A comparative measurement of the MAS signal of $CsHSO_4$-II collected at 300, 3000, and 30 000 s (not shown) revealed a large increase in the signal intensity between the 300 and 3000 s measurements but no further increase with increasing delay time to 30 000 s, further supporting the conclusion that 3000 s is a sufficient delay time, while indicating that 300 s is not.

Overall, the ^1H MAS NMR spectra are similar to those reported by Hayashi and Mizuno[23] in terms of both peak positions and peak widths. In contrast to earlier work, however, no peak at ~8.2 ppm, attributed by Hayashi and Mizuno to surface-sorbed water, is observed here. In the present case, the use of crushed single-crystal samples (examined almost immediately after grinding) eliminates this peak, a straightforward strategy that has also proven effective for CsH_2PO_4.[32] It is also noteworthy that, in Hayashi and Mizuno's study, slight differences in the spectra were observed when the repetition delay time was changed from 10 to 100 s, indicating a long relaxation and the importance of long repetition delay times for quantitative study.

Direct measurements of the spin−lattice relaxation times through inversion−recovery measurements are presented in Figure 7 for both phases II and III of $CsHSO_4$. The signal intensity, $M_z(\tau)$, was fit to the expression[33]

$$M_z(\tau) = M_0\left[1 - 2\beta \exp\left(\frac{\tau}{T_1}\right)\right] \qquad (7)$$

where M_0 is the thermal equilibrium intensity, τ is the measurement time, T_1 is the spin−lattice relaxation time, and β is a parameter, required to be less than or equal to 1, describing possible nonexponential relaxation behavior. Where the fitted value of β became greater than 1, it was replaced by unity. The data indicate T_1 times of 730 ± 80 and 246 ± 12 s for phases III and II, respectively. While these are rather long relaxation times in comparison to those of organic compounds and even in comparison to previous measurements of $CsHSO_4$ (~100 s as reported by Mizuno and Hayashi[34] and by Damyanovich et al.[35] and ~15 s as reported by Compton et al.[36] and by Hayashi and Mizuno[23]), the relatively low proton concentration and thus limited proton−proton interactions in $CsHSO_4$ are consistent with the results obtained here. Indeed,

(29) Klug, H. P.; Alexander, L. E. *X-Ray Diffraction Procedures for Polycrystalline and Amorphous Phases*, 2nd ed.; John Wiley and Sons: New York, 1974; p 656.
(30) Eckert, H.; Yesinowski, J. P.; Silver, L. A.; Stolper, E. M. *J. Phys. Chem.* **1988**, *92*(7), 2055–2064.
(31) Bloembergen, N.; Purcell, E. M.; Pound, R. V. *Phys. Rev.* **1948**, *73* (7), 679–712.
(32) Boysen, D. A.; Haile, S. M.; Liu, H. J.; Secco, R. A. *Chem. Mater.* **2003**, *15*(3), 727–736.
(33) Fukushima, E.; Roeder, S. B. W. *Experimental Pulse NMR: a Nuts and Bolts Approach*; Addison-Wesley Publishing Co.: Reading, MA, 1981; p 169.
(34) Mizuno, M.; Hayashi, S. *Solid State Ionics* **2004**, *167*(3−4), 317–323.
(35) Damyanovich, A.; Pintar, M. M.; Blinc, R.; Slak, J. *Phys. Rev. B* **1997**, *56*(13), 7942–7946.
(36) Compton, M. G.; Maynes, K. C.; Pavelites, J.; Baker, D. B. *Solid State Commun.* **2005**, *136*(3), 138–141.

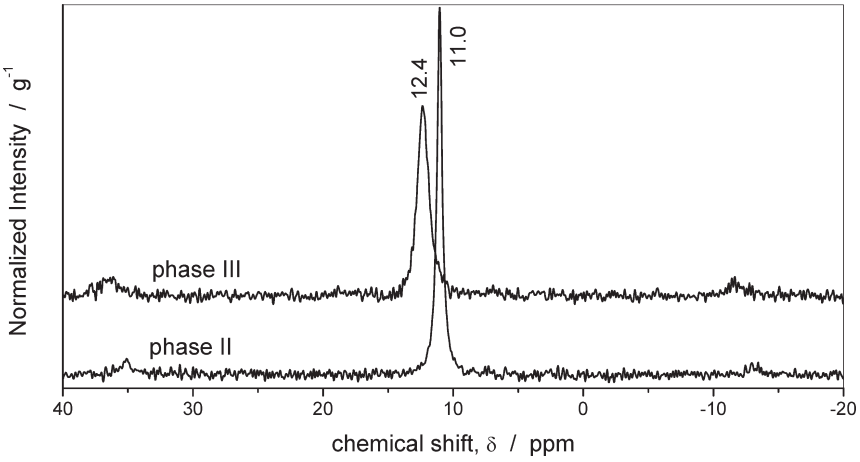

Figure 6. ^{1}H MAS NMR spectra for $CsHSO_4$. The chemical shifts are referenced to TMS. Peaks at chemical shifts of ~35 and ~−12 ppm are spinning side bands.

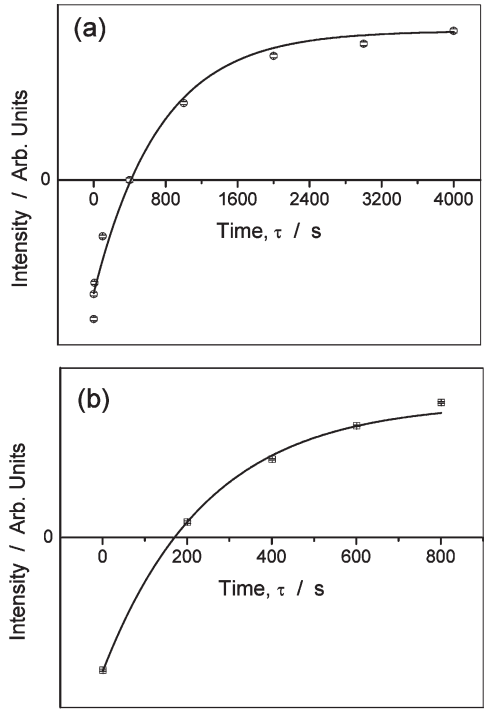

Figure 7. ^{1}H NMR inversion−recovery measurement for (a) neat $CsHSO_4$-III and (b) $CsHSO_4$-II. Points are the integrated peak intensities as a function of the measurement time, and the curves are the fit to the expression given in eq 7, with β fitted as 0.89 ± 0.10 for part a and fixed at 1 for part b. Error bars for measured data fall within the size of the data points.

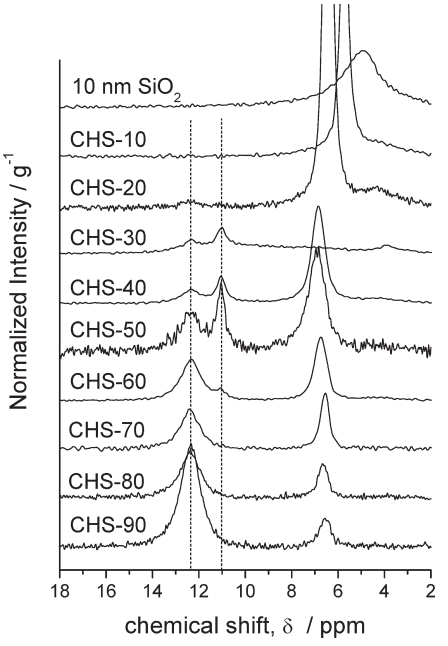

Figure 8. ^{1}H MAS NMR spectra for $CsHSO_4$−SiO_2 composites and neat SiO_2. The chemical shifts are referenced to TMS. Lines indicate chemical shift values of 12.4 and 11.0 ppm, corresponding to phases III and II, respectively, of crystalline $CsHSO_4$.

Mizuno and Hayashi have estimated that, considered alone, dipolar contributions to the relaxation would lead to a T_1 of over 10^5 s at a field strength of 200 MHz (and a factor of ~6 increase in T_1 would result from the higher field of 500 MHz used here[34]). Furthermore, the measurement times utilized here are much longer than those typically employed (to 800 s for phase II and to 4000 s for phase III), and experiments that are too short in duration can yield artificially short relaxation times.

The ^{1}H MAS NMR spectra for the composites are presented in Figure 8. The spectra show that peaks occur at chemical shifts corresponding precisely to the two phases of $CsHSO_4$ and showing the greater peak broadening for phase III. In general, the peak intensity for phase III decreases with increasing SiO_2 content, consistent with the powder XRD data. Additional peaks in the vicinity of 5−7 ppm are attributed to protons incorporated into the amorphous $CsHSO_4$ and/or into the silica itself. In the case of SiO_2 alone, a single peak at 5 ppm is observed. For samples with 40% and higher $CsHSO_4$ content, the peak appears in the region 6.5−7 ppm and moves toward higher chemical shift values with increasing silica content until high concentrations of SiO_2 are reached, suggesting a gradual change in the chemistry of the amorphous $CsHSO_4$ with changes in the overall system composition. In addition, the peak intensity generally increases with increasing SiO_2 content, consistent with the diffraction data analysis. However, because the

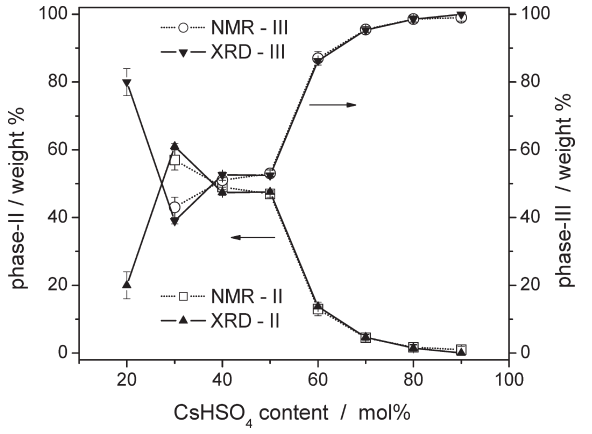

Figure 9. Relative amounts of phases II and III within the crystalline portion of $CsHSO_4$ in the $CsHSO_4-SiO_2$ composites. Comparison of the results obtained by XRD (Rietveld refinement) and by NMR (ratio of the integrated peak intensities). For CHS-20, the quantity of crystalline $CsHSO_4$ is low, and only the XRD estimate is included.

proton content (and even the chemical environment) in the amorphous region is expected to depend sensitively on the details of the sample history subsequent to synthesis and humidity levels under ambient measurement conditions, no attempt is made here to use either the peak positions or integrated intensities of the NMR peaks for quantitative analysis of the amorphous content or chemical nature. The anomalous behavior of sample CHS-30 is believed to be due to these factors.

In contrast, because the peaks at 11.0 and 12.4 ppm correspond to crystalline phases, their positions do not change for different samples. Moreover, their integrated intensities can be expected to be directly proportional to the quantity of the phase present in the sample. Indeed, the relative amounts of the two phases implied by the integrated NMR peaks (evaluated using a Gaussian profile) correspond, almost precisely, to the relative amounts of these two phases given by the diffraction analysis (Figure 9). In the case of the CHS-20 sample, it is apparent that, despite the low quantity of the crystalline phase and hence the impossibility of peak fitting, the amount of phase III exceeds that of phase II, as in the case of the XRD data.

Turning to the proton relaxation behavior in the composites, the inversion−recovery data for a representative composite sample, CHS-60, are shown in Figure 10, where the behavior of all three types of protons (phase III with a chemical shift of 12.4 ppm, phase II with a chemical shift of 11.0 ppm, and the amorphous region with a chemical shift of 6.7 ppm) has been measured. The protons occurring in phase III within the composite retain very long relaxation times, with $T_1 = 690 \pm 160$ s, and the measurements of other composites fall between this value and the value of 730 s noted for neat $CsHSO_4$-III. In contrast, the spin−lattice relaxation time for phase II decreases by a remarkable 4 orders of magnitude, becoming only 0.170 ± 0.010 s when in the composite. As in the case of the diffraction data, this result indicates that $CsHSO_4$-II obtained in the composite is highly influenced by the presence of SiO_2, whereas $CsHSO_4$-III is not. One

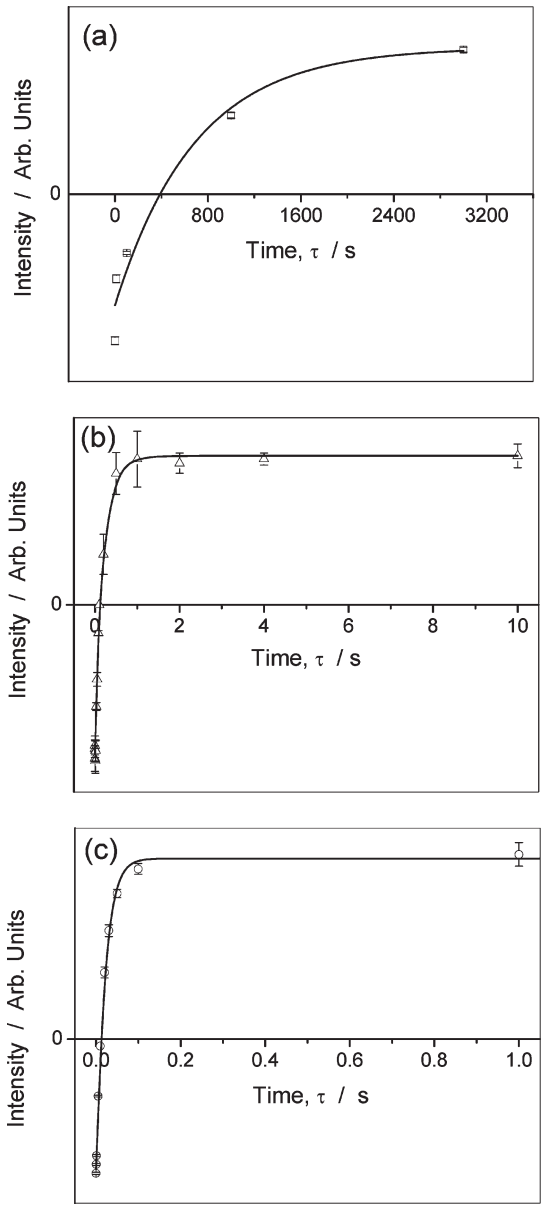

Figure 10. ^{11}H NMR inversion−recovery measurement for CHS-60 for peaks with chemical shifts of (a) 12.4 ppm, corresponding to $CsHSO_4$-III, (b) 11.0 ppm, corresponding to $CsHSO_4$-II, and (c) 6.7 ppm, corresponding to the amorphous region of the composite. Points are the integrated peak intensities as a function of the measurement time, and curves are the fit to the expression given in eq 7, with β fitted as 0.89 ± 0.10 for part a, fixed at 1 for part b, and fitted as 0.86 ± 0.12 for part c.

possible source of the influence is through a decrease in the $CsHSO_4$-II particle size in the presence of SiO_2 or, albeit less likely, the result of paramagnetic impurities in the silica that shorten the spin−lattice relaxation time in both $CsHSO_4$-II and the silica itself. In the case of the proton associated with the amorphous region, T_1 is even shorter, only 0.020 ± 0.001 s, a value comparable to that also observed in the as-purchased silica (not shown).

Discussion

The powder XRD and NMR data clearly show that aqueous precipitation of $CsHSO_4$ in the presence of SiO_2 nanoparticles leads to crystallization of the otherwise metastable phase II of $CsHSO_4$ along with a substantial

degree of amorphization of $CsHSO_4$. Because the X-ray data measure the proportion of $CsHSO_4$ that is "lost" to amorphization, they are insensitive to the water content in the amorphous region and hence provide a highly reliable measure of amorphization. The overall phase behavior is summarized in Figure 11, from which the influence of SiO_2 on the crystallization of $CsHSO_4$ is readily apparent: at high silica content, $CsHSO_4$ is fully amorphized, at intermediate content, all three forms of $CsHSO_4$ are present, and eventually at low SiO_2 content, the thermodynamically stable $CsHSO_4$-III becomes the predominant phase. Furthermore, as noted above, the broadening of the diffraction peaks suggests that the $CsHSO_4$-II particle size in composites in which this phase is present is on the order of 35−45 nm.

From these results, we propose that the composite systems adopt a microstructure as shown schematically in Figure 12, in which SiO_2 particles serve as the nucleation site for $CsHSO_4$ precipitation. The material directly in contact with SiO_2 is amorphized and may be chemically incorporated into the silica; that in contact with the amorphous solid acid (or solid acid containing silica) adopts the phase II crystalline structure and grows to dimensions of only ~40 nm, as either isolated particles or a continuous layer. The chemical state of the protons in this nanometric $CsHSO_4$-II is markedly different from that in bulk $CsHSO_4$-II, as reflected in the dramatically smaller T_1 relaxation time in the former. Simultaneous with heterogeneous precipitation of $CsHSO_4$ on the surface of SiO_2, a portion of the solid acid precipitates without influence from silica, adopts the usual phase III crystalline structure, and retains the long spin−lattice relaxation time of neat $CsHSO_4$-III. These crystallites of phase III grow to macroscopic dimensions, typical of precipitation from solutions free of SiO_2. Preliminary scanning electron microscopy (SEM) imaging indicates that the $CsHSO_4$-covered SiO_2 nanoparticles become agglomerated and distributed over the surface of the larger phase III particles, presumably as a result of van der Waals interactions.

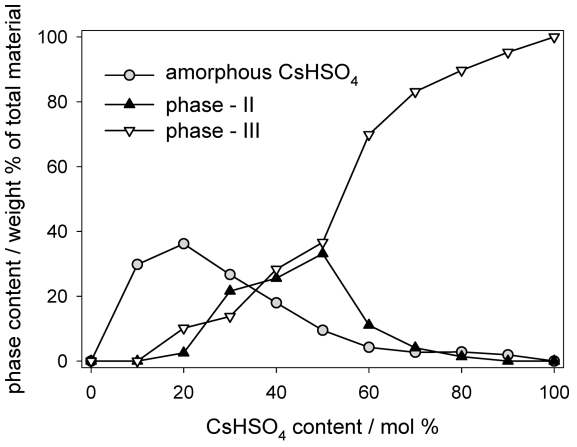

Figure 11. Summary of the phase behavior in $CsHSO_4$−SiO_2 composites, showing the phase content of the three different forms of $CsHSO_4$ (relative to the weight of the total material) as a function of the overall composite composition.

In composites with very small molar fractions of $CsHSO_4$ (e.g., CHS-10), the entirety of the acid salt is apparently consumed in the amorphous region. As the amount of $CsHSO_4$ is increased, "normal" precipitation of $CsHSO_4$-III competes with the incorporation of $CsHSO_4$ into the amorphous phase, and it is only when the $CsHSO_4$ content exceeds a certain threshold, specifically, ~20 mol %, that $CsHSO_4$-II is observed. At this composition, which corresponds to ~50 wt % $CsHSO_4$, over 85% of the entire sample mass is amorphous, 10.5 wt % crystallizes as phase III and just 2.5 wt % crystallizes as phase II.

Overall, the observation of a high degree of amorphization in high SiO_2 content composites is consistent with previous suggestions in the literature, although complete quantification has not been provided in those earlier studies. The high degree of amorphization may be responsible for high conductivity at temperatures below the superprotonic transformation at 141 °C. However, as reported by Ponomavera and colleagues,[37−39] for example, such composites display in a negligible increase in conductivity at the transition and thus lower conductivities at high temperatures than those with lower SiO_2 contents. While the processing of the materials and choice of SiO_2 in those studies differ from what has been

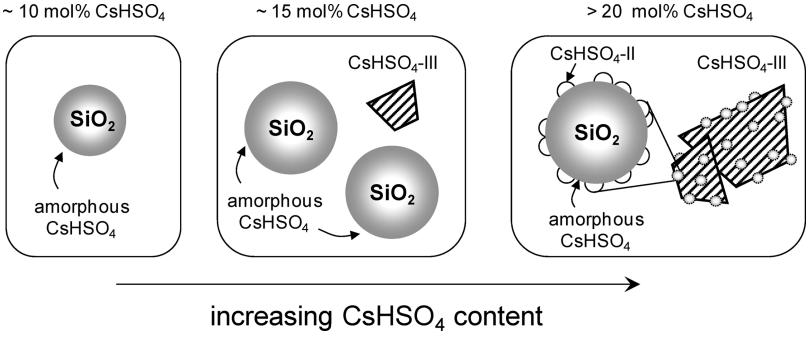

Figure 12. Schematic (not to scale) of the phase distribution in $CsHSO_4$−SiO_2 composites. At small concentrations of $CsHSO_4$, the entirety of the solid acid is incorporated onto the surface of the silica in the form of an amorphous phase. A small increase in the $CsHSO_4$ concentration increases the amount of amorphous $CsHSO_4$ but also leads to the direct precipitation of phase III. At higher $CsHSO_4$ concentrations, the amorphous $CsHSO_4$ serves as a nucleation size for phase II precipitation, while an increasing portion of the solid acid precipitates as phase III, independent of the silica nanoparticles. Preliminary SEM imaging suggests that the SiO_2−$CsHSO_4$-II particles are distributed as agglomerates over the surface of the larger phase III particles. At the highest $CsHSO_4$ amounts, the phase III material dominates over the amorphous and phase II forms of $CsHSO_4$.

examined here, the absence of a signature of superprotonic behavior is not surprising, if those composites, like the ones of this work, have the majority of the solid acid incorporated as an amorphous phase.

Summary

The influence of nanoparticulate SiO_2 on the crystallization behavior of $CsHSO_4$ from aqueous solution has been quantitatively evaluated. From XRD analysis, it is shown that SiO_2 induces amorphization of a portion of the $CsHSO_4$ and the crystallization of the otherwise metastable phase II. While both amorphization and the occurrence of phase II in such composites have been previously suggested in the literature,[40] the extent has not previously been fully quantified, nor have the phenomena been observed for nonporous SiO_2. Thus, the interaction between $CsHSO_4$ and SiO_2 has a chemical rather than mechanical origin and, furthermore, does not require high temperature treatment to occur. The phase distribution was found to be stable for over one year, indicating the strength of the stabilization effect that SiO_2 has on phase II of $CsHSO_4$. The NMR studies show MAS ^1H chemical shifts of 11.0 and 12.4 ppm, respectively, for phase-II and phase-III of $CsHSO_4$, values that are consistent with expectations based on the O···O distances in the respective hydrogen bonds and with previous reports. In contrast to previous studies, however, the spin−lattice relaxation times are found to be very long (as much as $\sim$ 730 s in phase III), and apparently result from the low total density of dipolar elements. The MAS ^1H peak shifts are retained in the composite systems, and excellent agreement is observed between the $CsHSO_4$ phase quantities implied by the integrated intensities of the MAS ^1H peaks and the Rietveld refinement of the X-ray phase fractions. Additional peaks at smaller chemical shifts (5−7 ppm) in the SiO_2 rich composites are attributed to the amorphized $CsHSO_4$ and to H_2O incorporated into the silica. Furthermore, while the long T_1 is retained for phase-III in the composite, that of phase-II is decreased by a remarkable 4 orders of magnitude.

The overall microstructural picture that emerges from these studies is a system in which SiO_2 particles either incorporate or are covered with an amorphous coating of $CsHSO_4$-like material. These amorphous particles serve as nucleation sites for nanoparticulate $CsHSO_4$-II, which then coexists with independently nucleated particles of $CsHSO_4$-III. In composites with small molar fractions of $CsHSO_4$ (up to 10 mol %), the entirety of the acid salt is consumed in the amorphous region. As the amount of $CsHSO_4$ is increased, "normal" precipitation of $CsHSO_4$-III competes with the incorporation of $CsHSO_4$ into the amorphous phase, and it is only when the $CsHSO_4$ content exceeds a certain threshold that $CsHSO_4$-II is observed. At high $CsHSO_4$ content, the extent of amorphization becomes negligible, as does the extent of crystallization in metastable phase II.

Acknowledgment. The authors gratefully acknowledge support from the National Science Foundation (Grant DMR-0435221) and via the Caltech Center for the Science and Engineering of Materials (Grant DMR-0520565). Dr. Sonjong Hwang of the California Institute of Technology has kindly assisted with the acquisition of NMR data. We also thank Dr. Clare Grey of SUNY Stonybrook for valuable discussions.

Appendix

The background evaluation was performed using an iterative procedure as implemented in the *X'pert Plus* commercial software package. Specifically, approximately 5% of the data (every 20 data points) are used to generate a first approximation of the background. For those instances in which the selected point corresponds to a position within a diffraction peak, the value of the background at that position is replaced by the mean value of the background at the two neighboring points. The background intensity profile is iteratively determined by comparing the intensities at position i, b_i to $m_i + c$, where m_i is the mean background intensity of the two neighboring points $i + 1$ and $i - 1$ and c is a constant that accounts for local curvature in the background, and then replacing b_i with m_i whenever $b_i > m_i + c$. The procedure converges within 30 iterations for typical diffraction patterns. The modified diffraction patterns for Rietveld refinement are obtained after subtraction of b_i and then addition of a constant background term equal to the lowest value of b_i. A nonzero background intensity is required to prevent the occurrence of zero intensity points that could otherwise give rise to singularities in the refinement process.

(37) Ponomareva, V. G.; Lavrova, G. V. *Solid State Ionics* **2001**, *145* (1−4), 197–204.
(38) Ponomareva, V. G.; Lavrova, G. V.; Simonova, L. G. *Solid State Ionics* **1999**, *119*(1−4), 295–299.
(39) Ponomareva, V. G.; Uvarov, N. F.; Lavrova, G. V.; Hairetdinov, E. F. *Solid State Ionics* **1996**, *90*(1−4), 161–166.
(40) Burgina, E. B.; Ponomareva, V. G.; Baltahinov, V. P.; Kostrovsky, V. G. *J. Struct. Chem.* **2005**, *46*(4), 608–618.